Chapter 2

A Cooperative Shear Model for the Rheology of Glass-Forming Metallic Liquids

Key words: Amorphous metals, Non-Newtonian flow, Shear transformation zones, Ultrasonic measurement, Compression test

2.1 Abstract

A rheological law based on the concept of cooperatively sheared flow zones is presented, in which the effective thermodynamic state variable controlling flow is identified to be the isoconfigurational shear modulus of the liquid. The law captures Newtonian as well as non-Newtonian viscosity data for glass-forming metallic liquids over a broad range of fragility. Acoustic measurements on specimens deformed at constant strain rate correlate well with the measured steady-state viscosities, hence verifying that viscosity has a unique functional relationship with the isoconfigurational shear modulus.

2.2 Introduction

In a normal metal the atoms are arranged in an orderly crystalline arrangement. In a metallic glass the liquid has been rapidly undercooled to the point at which nucleation and growth of crystals has been arrested. Therefore, the amorphous structure of the liquid is retained even at room temperature, resulting in a glass. There are several interesting phenomena associated with this amorphous structure. The deformation mechanisms that exist in normal metals do not occur in metallic glasses. This results in high strengths and large elastic limits. Furthermore, there is an apparent glass transition temperature and crystallization temperature in contrast to the normal melting temperature associated with crystalline metals. Additionally, between the glass transition and crystallization temperatures, metallic glasses flow plastically due to a decrease in the viscosity of the material. This is due to increased kinetic rates of the material with increasing temperature [1].

A map of these high-temperature deformation processes can be constructed using viscosity measurements. The deformation processes can be grouped into three distinct modes. The first mode is Newtonian flow, in which the viscosity is purely a function of the temperature and is insensitive to strain rate. The next type of flow is non-Newtonian flow, in which viscosity decreases with increasing strain rate. Both of these modes result in homogenous deformation of the specimen. The last type of deformation is shear localization. In shear localization, flow is isolated in a shear band that may propagate catastrophically through the specimen. A map of these processes has been presented in Ref. [2] for the Vitreloy 1 system.

Over the last three decades, several phenomenological theories have been proposed to explain the behavior of metallic glasses in these different flow regimes. Most of these theories are founded on two hypothetical flow mechanisms: dilatation [3] and cooperative shear[4]. By analogy to granular materials, metallic glasses were thought to flow by deformation-induced dilatation, which results in creation of microstructural "free volume," leading to flow localization and consequent softening [3]. Owing to their ability to effectively capture the flow characteristics of metallic glasses, free volume models have been regarded as good phenomenological flow models and have been widely embraced.

Even though experimental assessment of excess molar volume provided certain evidence of deformation-induced dilatation [5, 6], it has not been possible to quantitatively link measurable free volume to flow as predicted by free volume models. To some extent, this can be attributed to the lack of a fundamental thermodynamic definition of "free volume," leading to constitutive models that possibly lack thermodynamic consistency. This is due to the inability to distinguish the free volume contributions from thermal, pressure, and configurational effects separately. In an alternative approach [4], flow in amorphous metals was thought to be accommodated by cooperative shearing of atomic clusters, referred to as "shear transformation zones." In this theory it was envisioned that the small clusters of atoms in the material become plastically and mechanically polarized due to an applied stress field. As more of those clusters are formed, the "shear transformation zones" begin to interact and cooperatively deform. It was also envisioned that the unrelaxed clusters were responsible for the anelastic responses seen in metallic glasses.

In a recent study [7], it has been shown that plastic yielding in metallic glasses can be effectively accounted for by adopting a cooperative yielding analysis for these flow zones similar to the one developed by Frenkel [8] for dislocation-free crystals. In the present study, we employ that analysis to investigate the rheology of metallic-glass-forming liquids.

2.3 Experimental

Viscosity tests were performed on $Pd_{43}Ni_{10}Cu_{27}P_{20}$. Additionally, ultrasonic measurements were performed on $Pd_{43}Ni_{10}Cu_{27}P_{20}$ and $Zr_{41.2}Ti_{13.8}Ni_{10}Cu_{12.5}Be_{22.5}$ in order to obtain the isoconfigurational shear modulus.

$Pd_{43}Ni_{10}Cu_{27}P_{20}$ [9] alloy was made by first prealloying a mixture of Pd, Ni, and Cu. The prealloying was accomplished using induction heating. The process was carried out in a quartz tube under an inert argon atmosphere. The prealloy was then combined with P and sealed under an argon atmosphere in a quartz tube. The alloy was then heated at 0.1 K/min up to 1023 K and allowed to cool back to room temperature. The $Pd_{43}Ni_{10}Cu_{27}P_{20}$ alloy was then fluxed with B_2O_3 at 1000 K for 1000 sec. The elements used in this process ranged in purity from 99.9 to 99.999%.

$Zr_{41.2}Ti_{13.8}Ni_{10}Cu_{12.5}Be_{22.5}$ [10] ingots were prepared from a mixture of elemental metals ranging in purity from 99.99 to 99.999%. The elements were alloyed in an induction melter with a water-cooled copper boat. An argon atmosphere was used during the alloying process. A titanium getter was used prior to alloying to scavenge any oxygen that was present.

After the alloys were prepared, the materials were cast into 4 mm diameter glassy rods of $Pd_{43}Ni_{10}Cu_{27}P_{20}$ for the viscosity tests and 6 mm diameter glassy rods of $Pd_{43}Ni_{10}Cu_{27}P_{20}$ and $Zr_{41.2}Ti_{13.8}Ni_{10}Cu_{12.5}Be_{22.5}$ for the shear modulus tests. The casting process was done under vacuum into a machined copper mold. The amorphous nature of the cast rods was verified by Differential Scanning Calorimetry and X-ray diffraction. The Differential Scanning Calorimetry was performed at a constant heating rate of 20

K/min. The machine used was a Netzch DSC 404C with graphite crucibles. The X-ray diffraction was performed on a Siemens Kristalloflex Diffractometer.

After verifying the amorphous nature of the specimens the rods were cut into 6 mm and 9 mm lengths respectively. Prior to testing it was necessary to ensure that the deformation surfaces were parallel. The top and bottom surfaces were ground perpendicular to the central axis of the specimens using a polishing jig and 600 grit sandpaper.

Isothermal viscosity measurements for $Pd_{43}Ni_{10}Cu_{27}P_{20}$ were obtained using parallel plate reheometry as done in Ref. [2]. Before taking viscosity measurements the specimens were allowed to thermally relax at the testing temperature. By assuming a Poisson ratio of 0.5 during plastic flow we can estimate the viscosity as

$$\eta = \frac{\sigma_{flow}}{3\dot{\varepsilon}}$$

where σ_{flow} is the flow stress in steady state and $\dot{\varepsilon}$ is the strain rate of the test. High-temperature compression tests were carried out on a Servo-Hydraulic Materials Testing System (MTS 358 Series). The MTS machine was equipped with multiple load cells including 5 kip, 20 kip, and 50 kip cartridges. There was a 5 in internal linear voltage displacement transducer (LVDT) that recorded the machine head displacement during testing.

An additional load frame was used during the testing of the metallic glass specimens. The load frame is described in detail in Figure 1 of Chapter 2 in Ref. [2]**.** The design includes an LVDT and its adapter, a split electric furnace, and a temperature feedback/control system. Small modifications such as increased insulation and increased

plate thickness for connecting the extension rods were incorporated into the current system.

The split furnace elements (#5010-1057-00A, Lunaire, WI) were half cylinders with an inner diameter of 75 mm and a length of 150 mm. The temperature control system incorporated a temperature controller (#CN77000) and two solid state relays (#SSR240DC25) from Omega Engineering. The temperature data from the sample was relayed to the temperature controller via a K-type thermocouple spot welded to the middle of the specimen. During the high-temperature compression tests the temperature controller was operated in the Proportional-Integral-Derivative mode [11]. The temperature controller maintained the specimen within ± 0.5 K of the programmed temperature. To insure that the temperature profile was uniform across the specimen, thermocouples were attached to different points along the specimen length for several tests. In those tests the different thermocouples registered less than 1 K difference between the top and bottom surfaces of the specimen. This is corroborated by looking at the thermal diffusivity of the material. A typical thermal diffusivity for metallic glasses is $5x10^{-6}$ m^2s^{-1} [12]. For a specimen with dimensions on the order of 4–6 mm the thermal relaxation time is on the order of several seconds. Hence, the specimens may be assumed to be at a homogeneous temperature for the performed strain rates.

The specimens were initially heated at 20 K/min. Upon reaching 20 K below the target temperature the temperature controller was switched to manual operation. Once in manual operation the target temperature was slowly approached to avoid any temperature overshoot. Once at the appropriate temperature the machine was again put into Proportional-Integral-Derivative mode, and the specimens were allowed to relax.

In addition to the viscosity measurements, we performed tests to measure the isoconfigurational shear modulus. In these tests we utilized specimens of $Zr_{41.2}Ti_{13.8}Ni_{10}Cu_{12.5}Be_{22.5}$ and $Pd_{43}Ni_{10}Cu_{27}P_{20}$ which have undergone mechanical deformation at constant strain rates and constant temperatures of 593 K and 548 K, respectively. Continuous-strain-rate compression tests were performed using the setup described above. In Ref. [13] the non-Maxwellian relaxation times (τ_{NM}) have been measured for $Pd_{43}Ni_{10}Cu_{27}P_{20}$. The measured relaxation times are around four times longer than the calculated Maxwellian relaxation times (τ_M) for $Pd_{43}Ni_{10}Cu_{27}P_{20}$. The Maxwellian relaxation time can be estimated as

$$\tau_M = \frac{\eta}{G}$$

Deformation was performed for a minimum of four τ_{NM} after a steady-state flow stress was attained. Upon unloading, quenching was performed as rapidly as possible in an effort to freeze the configurational state associated with the flow stress. The furnace was opened at the same time as the measurement was stopped. Once the furnace was opened the specimen was removed and quenched in water. The entire process took roughly 5 sec. The fastest sample relaxation time for which we attempted to "quench" in the configurational state was $\tau_M \approx 30$ sec. The amount of actual relaxation observed for such specimens with this τ_M was minimal. For longer relaxation times, relaxation during quenching was assumed to be negligible.

After quenching, the specimens were prepared for acoustic measurement. The specimens were polished to a 2 μm surface finish. To ensure the surfaces were parallel it was necessary to use a polishing jig that held the specimen's central axis perpendicular to

the polishing surface. We evaluated the shear modulus of the quenched unloaded specimens using ultrasonic measurements along with density measurements [14]. Shear wave speeds were measured at room temperature using the pulse-echo overlap setup described in [15]. 5 MHz transducers (Panametrics-NDT V157) and a computer controlled pulser/receiver (Panametrics-NDT Model 5800) were used to produce and measure the acoustic signal. The signal was measured using a Tektronix TDS 1012 oscilloscope. The data was captured using a routine developed by Mary Laura Lind in LabView.

The sound velocity was evaluated using the measured time delay of the acoustic signal and the length of the specimen. The time delay was measured in MatLab by matching the wave profiles from the first and last echo recorded, and then measuring the time between them. The specimen length was measured using calipers with an accuracy of ±0.005 mm. The sound velocity was calculated using:

$$c = \frac{2l(n-1)}{t}$$

where c is the sound velocity, l is the length of the specimen, t is the measured time delay, and n is the number of echoes measured. If there were four echoes and you compared the first and last echo n would equal 4. If the second and third echoes were compared, n would equal 2.

Densities were measured by the Archimedes method, as given in the ASTM standard C693-93. The weight measurements were carried out on a Mettler Toledo AG 204 Delta Range scale with an accuracy of ±0.00005 g. The water used was distilled water that had been degassed by bringing it to a gentle boil and then allowing it to cool to ambient temperature near the scale. The setup for measuring the weight of the specimens

under water included a 140 ml beaker which was filled with the degassed water. Inside the 140 ml beaker a smaller 10 ml beaker was freely suspended in the water using thin gauge Inconel wire less than 0.2 mm in diameter. The wire was attached to a frame that transmitted the load to the scale. Before weighing the samples the scale was zeroed for the initial load of the beaker and frame. Once the water was at ambient temperature the water temperature was recorded and the specimens were weighed. Additionally, the dry weight of each specimen was measured, and the air temperature was recorded. In determining the densities of the air and water a pressure of 760 mmHg was assumed when using the tables in the ASTM standard C693-93. The density was calculated using:

$$\rho = \frac{(W_A \rho_W - W_W \rho_A)}{(W_A - W_W)}$$

where W_A and W_W are the weight of the specimen in air and water respectively, and ρ_A and ρ_W are the densities of the air and water respectively.

After the sound velocity and density for a specimen was evaluated it was possible to estimate the isoconfigurational shear modulus using:

$$G = C^2 \rho$$

where C is the measured shear sound velocity at ambient conditions, and ρ is the density as determined above.

These room-temperature measurements were corrected to estimate the shear modulus at the temperature of the flow experiment by accounting for the Debye-Grüneisen temperature effect on the shear modulus of the frozen glass. The Debye-Grüneisen temperature effect is linked to the thermal expansion of the material. As the average atomic volume increases with increasing temperature the shear modulus of the

material softens. To correct the room-temperature measurements we utilized measured linear Debye-Grüneisen coefficients of 9 MPa/K for $Zr_{41.2}Ti_{13.8}Ni_{10}Cu_{12.5}Be_{22.5}$ [15] and 15 MPa/K for $Pd_{43}Ni_{10}Cu_{27}P_{20}$ [16]. The temperature correction was done using

$$G_{DG} = G_{RT} - (T_{Exp} - T_{RT})\frac{dG}{dT}_{DG}$$

where G_{DG} is the shear modulus corrected for the Debye-Grüneisen effect, G_{RT} is the shear modulus as measured at room temperature, T_{Exp} is the temperature of the deformation experiment, T_{RT} is room temperature, and dG/dT_{DG} is the measured linear Debye-Grüneisen coefficient

2.4 Discussion

There is a large amount of data in the literature detailing the viscosities of the different alloys shown in this chapter [2, 17-21]. Furthermore, the physical properties and processing routes for these alloys are well described [9, 10]. A discrepancy was found concerning the viscosity data for the $Pd_{43}Ni_{10}Cu_{27}P_{20}$ alloy. As seen in Fig. 2.1 there are almost two orders of magnitude difference between the viscosity data reported in Refs. [19, 20] and that reported in Ref. [21]. The viscosity as measured in Refs. [19, 20] is exceptionally low at the calorimetric glass transition temperature (T_g). A measurement of T_g is shown in Fig. 2.2. Even when accounting for the shifts of the calorimetric T_g with the different heating rate the viscosity of the undercooled liquid at that temperature should roughly be 10^{11} Pa-s to 10^{12} Pa-s. This discrepancy may be due to the difference in specimen size used in the test. In Refs. [19, 20] the specimens are 2 mm in diameter. In Ref. [21] the specimens are 5 mm in diameter. In order to resolve this problem the non-Newtonian viscosity regime was mapped out for different temperatures and strain rates for $Pd_{43}Ni_{10}Cu_{27}P_{20}$, and we compared the obtained Newtonian data to the data in the literature. The Newtonian measurements were found to fit with the data from Ref. [21] the best. This comparison can be seen in Fig. 2.3.

Following Ref. [7], a periodic energy density ϕ vs. strain γ can be formulated as $\phi/\phi_o = \sin^2\left(\pi\gamma/4\gamma_c\right)$, where ϕ_o is the barrier energy density, and γ_c is a critical shear strain limit shown to be a universal scale for metallic glasses. See Fig. 2.4 for an example of a potential energy well as modeled with this potential. This potential energy landscape can be viewed as arising from a collection of clusters where each cluster deforms to accommodate the applied stress field. These clusters are estimated to be

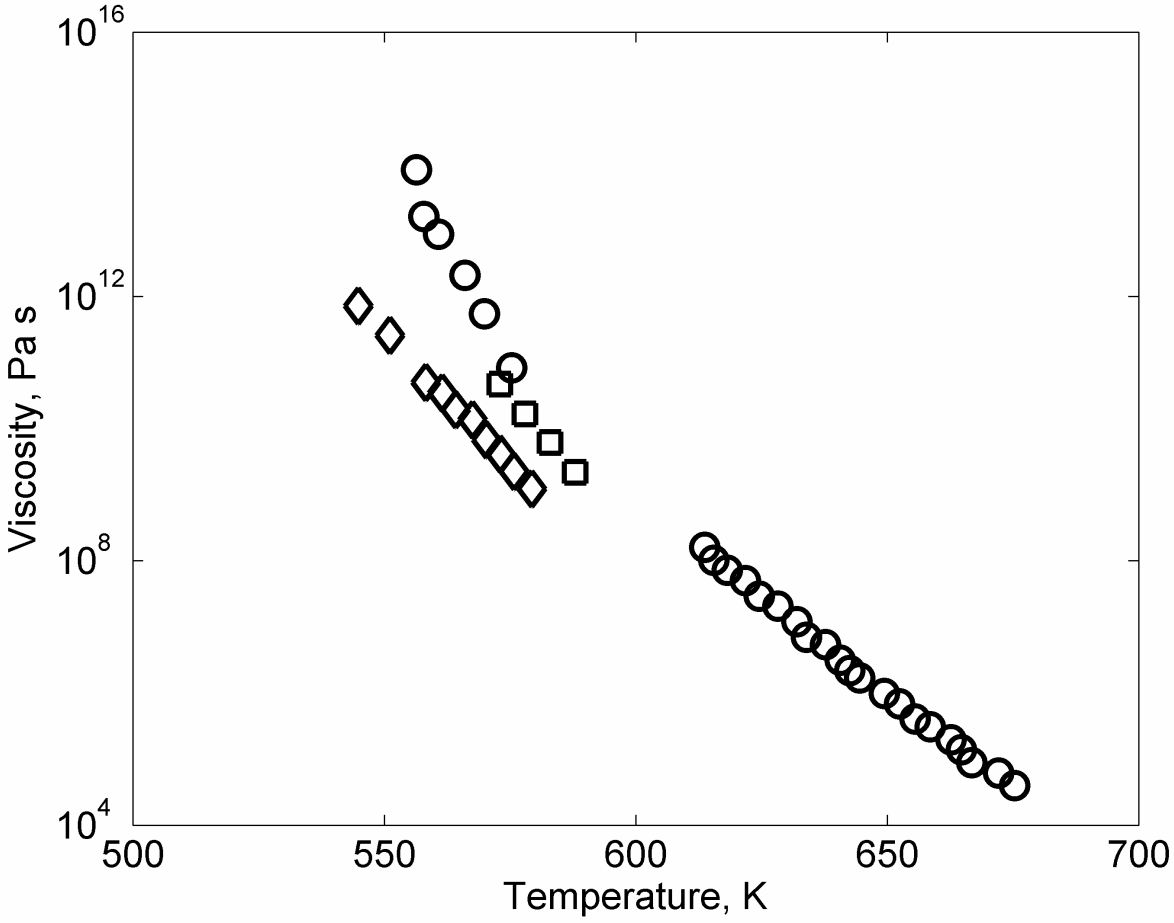

Figure 2.1. Conflicting Newtonian viscosity data for $Pd_{43}Ni_{10}Cu_{27}P_{20}$ obtained from references (◊) [19], (□) [20], and (O) [21].

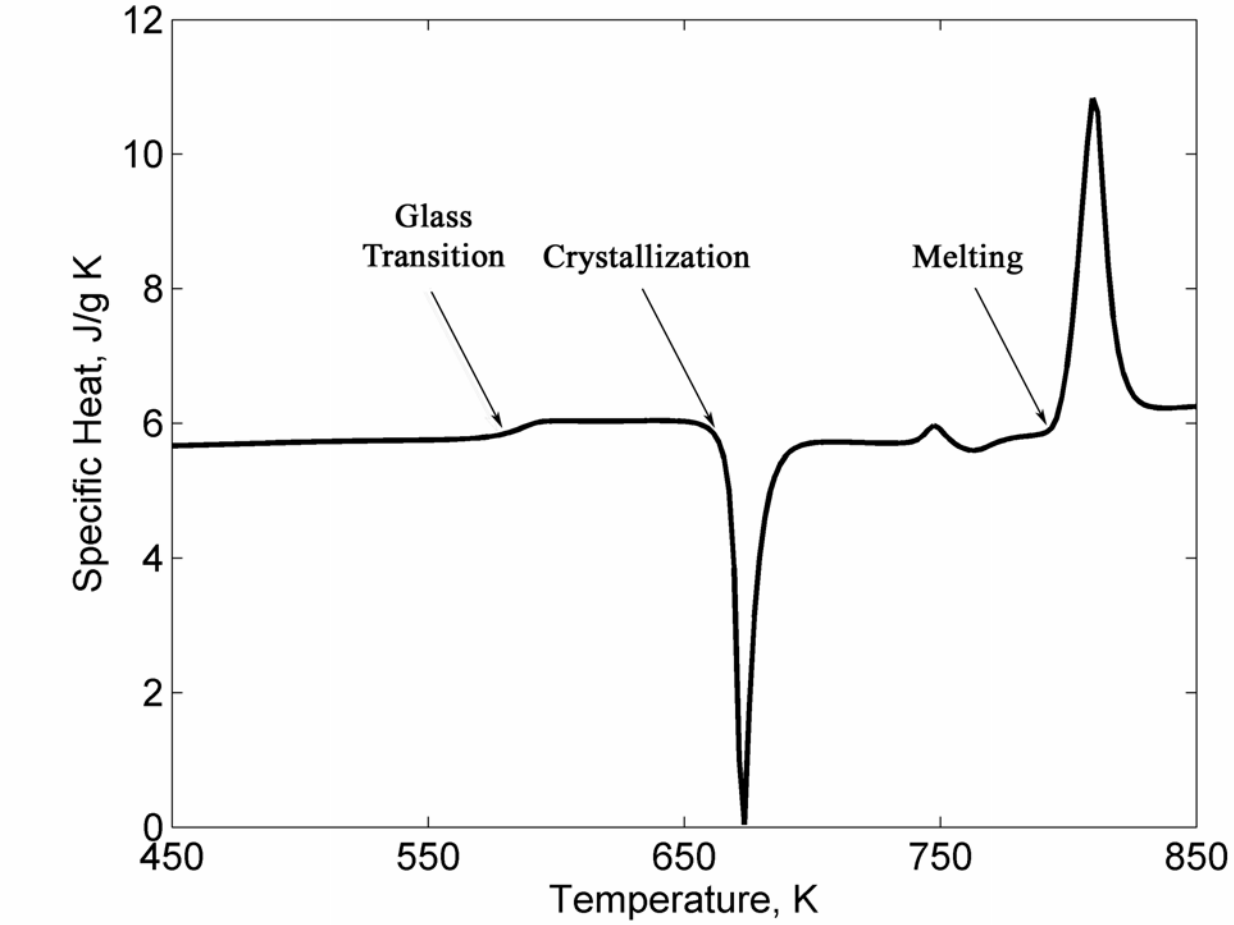

Figure 2.2. A Differential Scanning Calorimetry trace with a scan rate of 20 K/min for a $Pd_{43}Ni_{10}Cu_{27}P_{20}$ alloy. The calorimetric glass transition temperature is denoted in the figure.

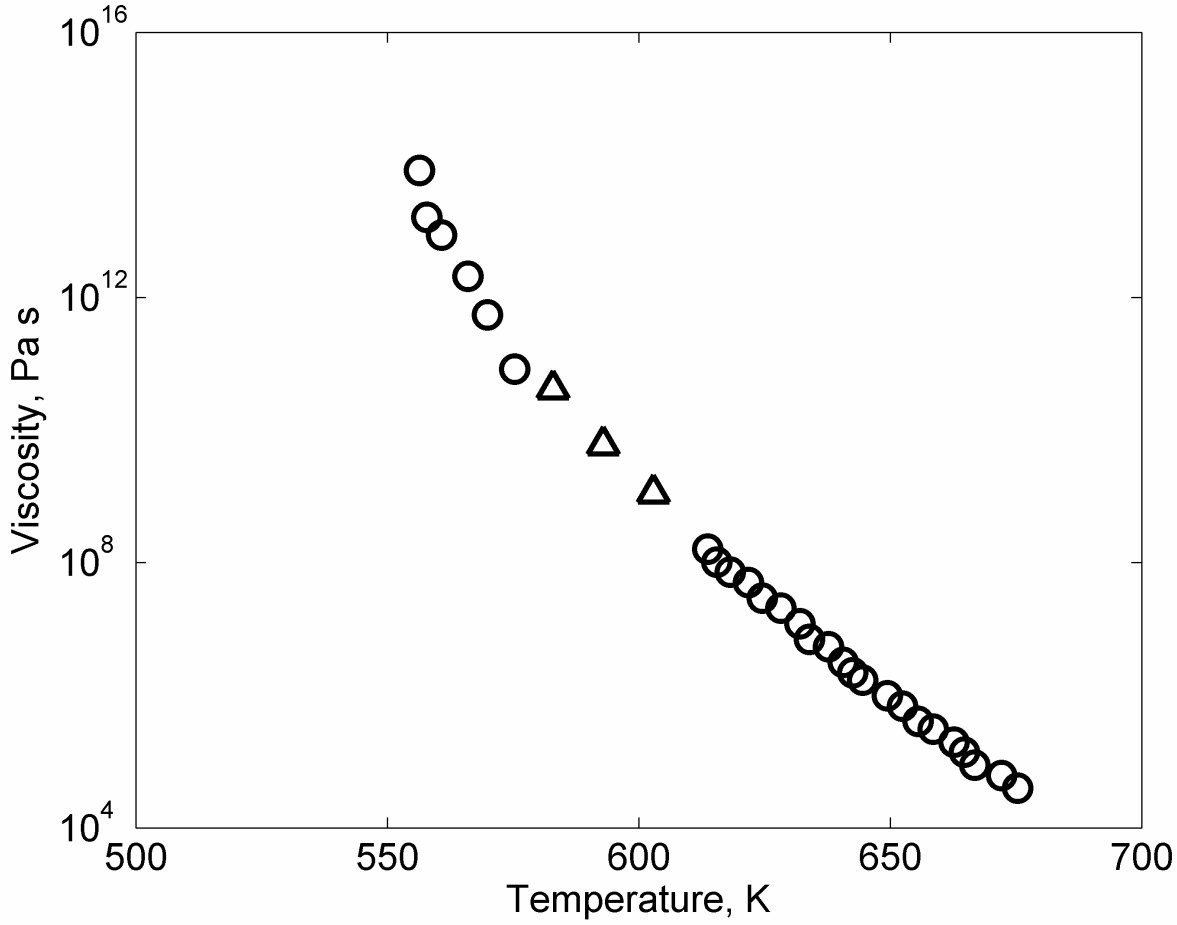

Figure 2.3. Newtonian viscosity data obtained from (Δ) experiments and (O) Ref. [21].

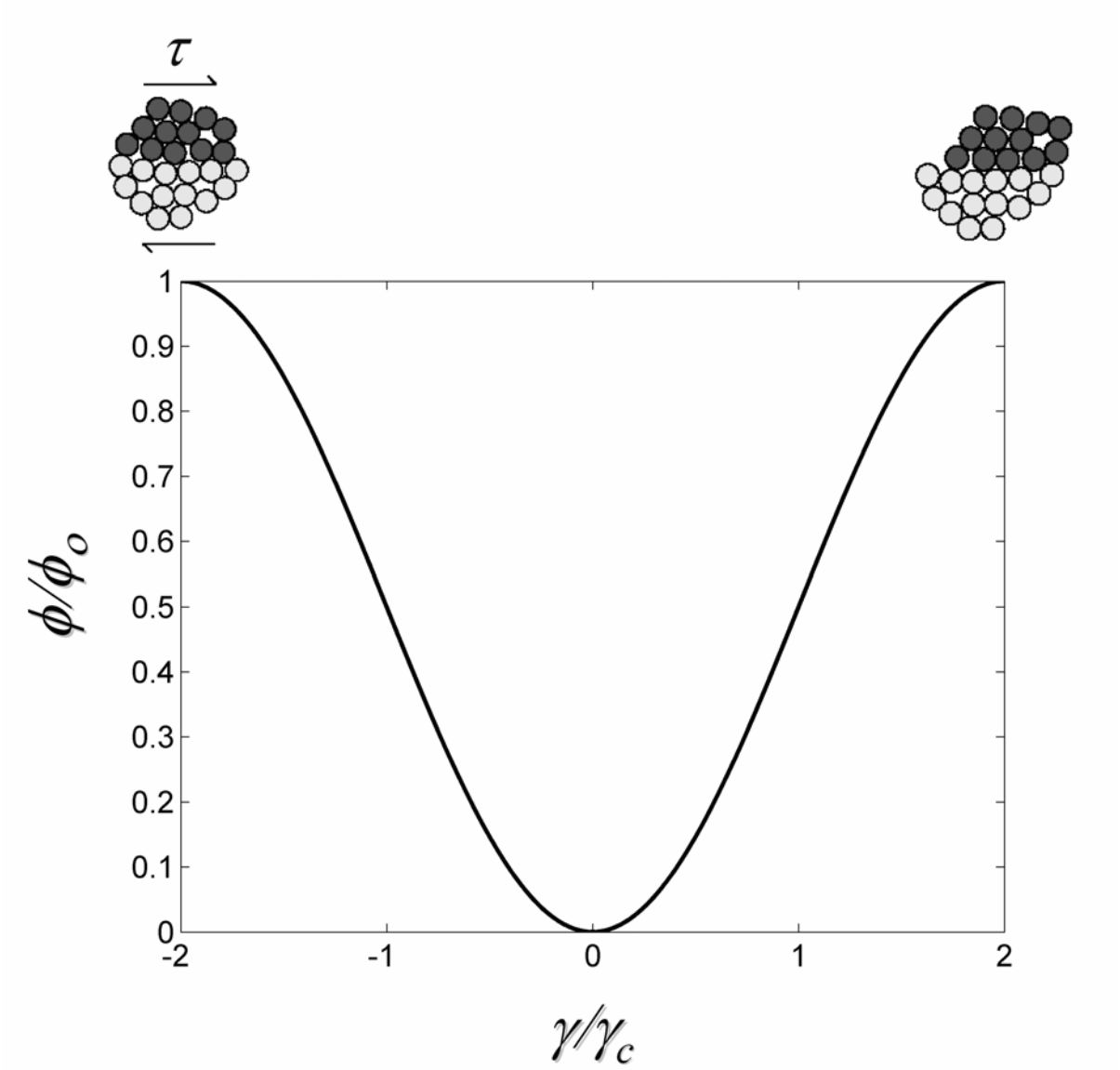

Figure 2.4. An example of the potential energy landscape generated from the function $\phi/\phi_o = \sin^2\left(\pi\gamma/4\gamma_c\right)$

~ 100–200 atoms in size, and are called Shear Transformation Zones (STZs) [7]. With this model the stress associated with moving a STZ out of the potential well can be calculated as $\tau(\gamma) = d\phi/d\gamma$. This results in the maximum shear stress occurring at $\gamma = \gamma_c$. Zero shear stresses occur at $\gamma = 0$ and $\gamma = 2\gamma_c$. Furthermore, the shear modulus is given by the curvature of the energy density function (i.e., $G = d^2\phi/d\gamma^2\big|_{\gamma=0}$), and a linear relationship between barrier energy density and shear modulus can be formulated as $\phi_o = \left(8/\pi^2\right)\gamma_c^2 G$. Multiplying by an effective zone volume Ω, the total energy barrier for configurational hopping between inherent states, which can be regarded as the activation barrier for shear flow, can be expressed as $W = \left(8/\pi^2\right)\gamma_c^2 G\Omega$. Acknowledging that the variables contributing to barrier softening are G and Ω, the expression for the energy barrier can be rearranged as $W = W_o\left(G/G_o\right)\left(\Omega/\Omega_o\right)$, where G_o and Ω_o are characteristic scales for the shear modulus and the zone volume, and $W_o \equiv \left(8/\pi^2\right)\gamma_c^2 G_o\Omega_o$. Taking the barrier crossing rate normalized by an attempt frequency to follow a Boltzmann distribution function, we can arrive at a viscosity law based on barrier softening:

$$\eta/\eta_\infty = \exp\left[W/kT\right] \tag{2.1}$$

where η_∞ is the Born-liquid limit of viscosity, which can be realized in the limit of $W \to 0$.

In the context of this analysis, Newtonian flow can be regarded as thermally activated flow where barriers are overcome entirely by thermal fluctuations. The viscosity should therefore be determined by the shear modulus and STZ volume corresponding to the equilibrium configurational state, G_e and Ω_e, whose temperature dependence we describe by an exponential decay function, as:

$$G_e/G_o = \exp\left(-nT/T_g\right)$$

and

$$\Omega_e/\Omega_o = \exp\left(-pT/T_g\right),$$

where T_g is the glass transition temperature. The form of this function originates from the probability distribution of inherent configurational states in a potential energy landscape model of a metallic glass [22]. In these expressions, n and p are indices quantifying the contributions of G and Ω to the softening of W. The equilibrium barrier therefore takes the form:

$$W_e = W_0 \exp\left[\ -(n+p)T/T_g\ \right].$$

Evaluating Eq. (2.1) at T_g we get:

$$W_g = kT_g \ln\left(\eta_g/\eta_\infty\right).$$

We are now able to define W_0 in reference to measurable quantities at the glass transition using:

$$W_0 = W_g \exp(n + p).$$

This results in:

$$W_e = kT_g \ln(\eta_g/\eta_\infty)\exp[\ (n + p)(1 - T/T_g)\ ].$$

Substituting W_e into Eq. (2.1), an equilibrium viscosity law is obtained where the only unknown is the combined fitting parameter, (n+p):

$$\frac{\eta_e}{\eta_\infty} = \exp\left\{\frac{T_g}{T}\ln\left(\frac{\eta_g}{\eta_\infty}\right)\exp\left[(n + p)\left(1 - \frac{T}{T_g}\right)\right]\right\}. \tag{2.2}$$

In Fig. 2.5, we present the fit of the equilibrium law to Newtonian viscosity data of metallic-glass-forming liquids. The law effectively captures the Newtonian viscosity of $Zr_{41.2}Ti_{13.8}Ni_{10}Cu_{12.5}Be_{22.5}$ [17] and $Pd_{40}Ni_{40}P_{20}$ [23-25] over the entire range of temperatures studied rheologically. Moreover, plotted on a normalized plot [26] (insert in Fig. 2.5), the law captures Newtonian data of liquids ranging from the strongest to the most fragile [21, 27-32], and can thus be perceived as a universal viscosity law. The fitting parameters are given in Table 2.1. By comparison to free-volume based laws, the one-parameter Cooperative shear model fits Newtonian data better than the two-

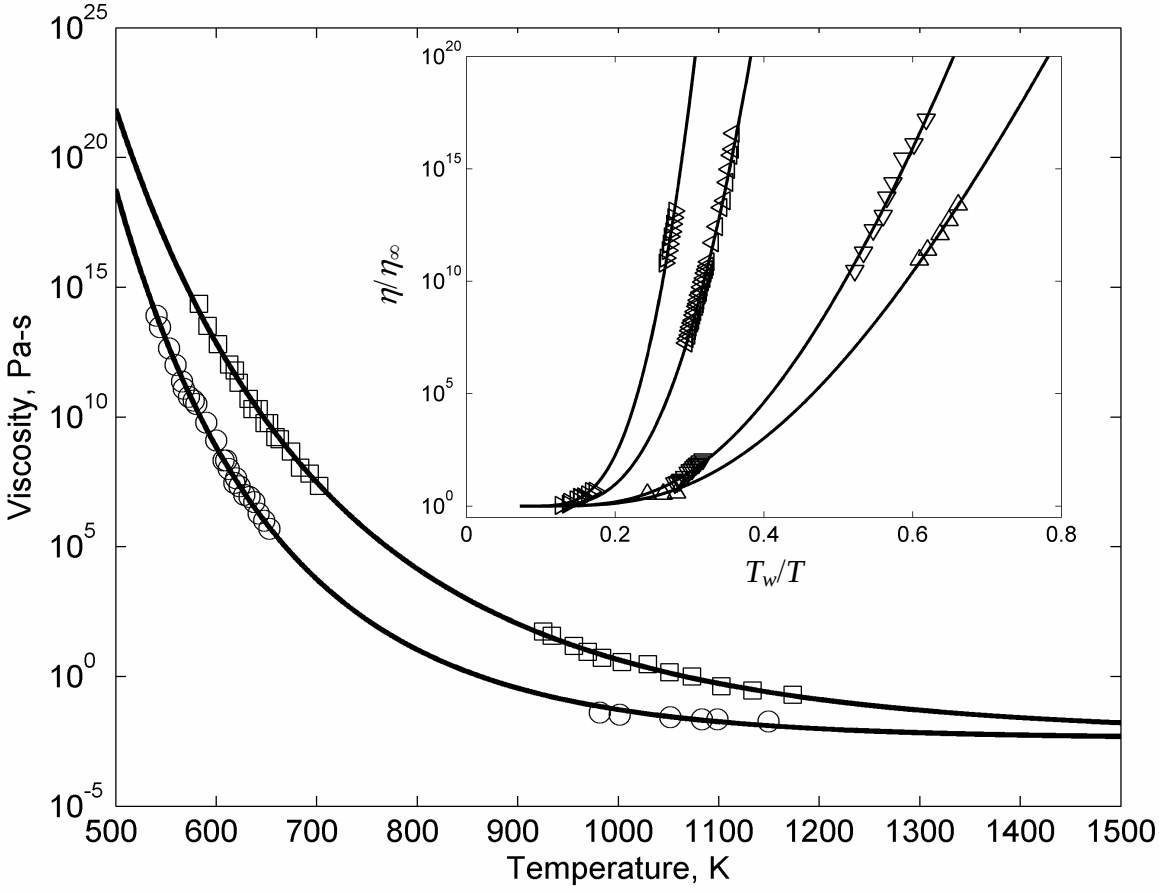

Figure 2.5. Fit of the equilibrium viscosity law, Eq. (3.1) and (3.2), to Newtonian data of metallic glass-forming liquids: $Zr_{41.2}Ti_{13.8}Ni_{10}Cu_{12.5}Be_{22.5}$ (□); $Pd_{40}Ni_{40}P_{20}$ (○); $Pd_{40}Ni_{10}Cu_{30}P_{20}$ (◁); $Pd_{77.5}Cu_6Si_{16.5}$ (▷); $La_{55}Al_{25}Ni_{20}$ (△); $Mg_{65}Cu_{25}Y_{10}$ (▽). Low-temperature viscosity data was produced by three-point beam bending, continuous-strain-rate tension and compression, and parallel-plate rheometry; high-temperature data was produced by concentric-cylinder rheometry, oscillating crucible, and electrostatic levitation [8-11,13-20].

parameter Vogel-Fulcher-Tammann law [33], and at least as well as the three-parameter Cohen-Grest law [34]. These fits are compared in Fig. 2.6.

	T_g [K]	$(n+p)$	η_∞ [Pa-s]
$Zr_{41.2}Ti_{13.8}Ni_{10}Cu_{12.5}Be_{22.5}$ [17]	613	1.75	5.6×10^{-3}
$Pd_{40}Ni_{40}P_{20}$ [23-25]	560	2.52	4.0×10^{-3}
$Pd_{43}Ni_{10}Cu_{27}P_{20}$ [13,Fig. 2.3]	569	2.85	2.2×10^{-3}
$Pd_{77.5}Cu_6Si_{16.5}$ [18,27]	635	3.53	1.0×10^{-2}
$La_{55}Al_{25}Ni_{20}$ [28,29]	450	1.43	5.3×10^{-4}
$Mg_{65}Cu_{25}Y_{10}$ [30,31]	405	1.72	1.5×10^{-3}

Table 2.1. Fit parameters to the equilibrium viscosity law, Eq. (2.1), for various metallic glass-forming liquids. It is noted that η_∞ was assigned a value near the Planck limit which resulted in a best fit (as typically implemented when fitting viscosity).

As evidenced from Fig. 2.5 and Table 2.1, fragile liquids are characterized by a high $n+p$, which suggests that liquid fragility is dictated by $n+p$, i.e., by the combined softening effects of G and Ω. From the functional dependencies of G and Ω, the relationship $(G/G_o)=(\Omega/\Omega_o)^{n/p}$ can be recognized, which leads to a correlation between G and W as $(G/G_o)=(W/W_o)^q$, where $q=n/(n+p)$. This can be reformulated in terms of the glass transition as $(G/G_g)=(W/W_g)^q$. A correlation between G and η may now be formulated as:

$$\frac{G}{G_g}=\left[\frac{T}{T_g}\frac{\ln(\eta/\eta_\infty)}{\ln(\eta_g/\eta_\infty)}\right]^q \tag{2.3}$$

where G_g is the isoconfigurational shear modulus at T_g. Equation (2.3) essentially states that variations in viscosity correlate uniquely to variations in shear modulus.

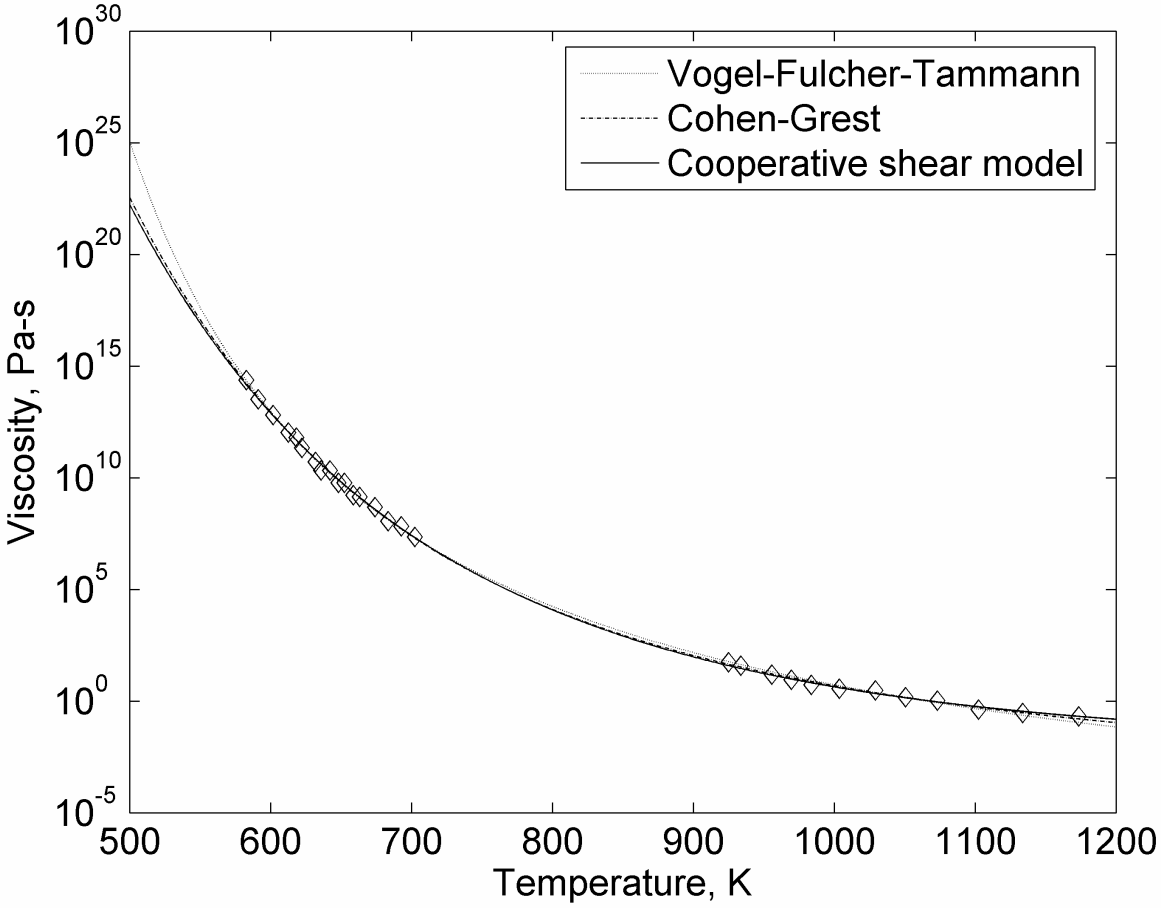

Fig 2.6. The two-parameter Vogel-Fulcher-Tammann law, three-parameter Cohen Grest law, and one-parameter Cooperative shear model are used to fit the Vitreloy 1 viscosity data from Ref. [17]. The fits have R^2 values of 0.9994, 0.9995, and 0.9995 respectively. From this comparison it is clear that the Cooperative shear model is capable of predicting the Newtonian viscosity of metallic glasses over a wide range of temperatures with the use of only one fitting parameter. Additionally, the one-parameter Cooperative shear model is found to have the same accuracy as the two- and three-parameter fitting laws.

We can now proceed to extend the softening law to the case of a driven system. A non-Newtonian flow law can be formulated by accounting for the effect of dissipated energy on W. This effect can be accounted for by considering the induced changes in the specific configurational potential energy of shear zones, ε. The rate of softening can thus be formulated as $\dot{W}_{sof} = \dot{\varepsilon}\,\delta W/\delta\varepsilon$, where $\dot{\varepsilon} \approx \eta\dot{\gamma}^2$ is the rate of production of specific configurational potential energy as a result of flow dissipation ($\dot{\gamma}$ is strain rate), and $\delta W/\delta\varepsilon = \left(\partial W/\partial T\right)/\left(\partial\varepsilon/\partial T\right)$ is a dimensionless thermodynamic parameter denoting changes in W with respect to changes in ε. Near T_g, we can differentiate $W_e = W_g \exp\left[\ (n+p)(1-T/T_g)\ \right]$ with respect to T at T_g to give $dW/dT\big|_{T_g} = -W_g(n+p)/T_g$. We can also evalute $\partial\varepsilon/\partial T \approx \left(\partial h/\partial T\right)\big|_{T_g}$, where h is the specific configurational enthalpy and $\left(\partial h/\partial T\right)\big|_{T_g}$ can be evaluated from enthalpy recovery experiments as Δc_p at T_g. Configurational relaxation can be accounted for by adopting a uni-molecular kinetic model as $\dot{W}_{rel} = \left(W - W_e\right)/\left(\alpha\tau_M\right)$, where $\tau_M = \eta/G = \eta/\left[\ G_g\left(W/W_g\right)^q\ \right]$ is the Maxwell relaxation time, and α is a model parameter quantifying the deviation from simple Maxwellian relaxation. Requiring $\dot{W}_{sof} = \dot{W}_{rel}$ for steady flow, we arrive at a self-consistent non-equilibrium law:

$$-\alpha\frac{(n/q)W_g}{T_g\Delta c_p}\eta\dot{\gamma}^2 = \frac{\left(W - W_e\right)\left(W/W_g\right)^q}{\eta/G_g}. \tag{2.4}$$

For $Zr_{41.2}Ti_{13.8}Ni_{10}Cu_{12.5}Be_{22.5}$, $G_e\left(T_g\right) \approx 33$ GPa [15] and $\left(\partial h/\partial T\right)\big|_{T_g} \approx 1.5$ MJ/m^{3}K [35], which gives $\delta W/\delta\varepsilon = -5.29\times10^{-28}$. For $Pd_{43}Ni_{10}Cu_{27}P_{20}$, $G_e\left(T_g\right) \approx 31$ GPa [16] and $\left(\partial h/\partial T\right)\big|_{T_g} \approx 2.5$ MJ/m^{3}K [36], which gives $\delta W/\delta\varepsilon = -5.32\times10^{-28}$. In Fig 2.7 we present the solution of Eq. (2.4), superimposed on the non-Newtonian data of $Zr_{41.2}Ti_{13.8}Ni_{10}Cu_{12.5}Be_{22.5}$ [18] and $Pd_{43}Ni_{10}Cu_{27}P_{20}$, produced by adjusting α to 16.5 and 58.5, respectively. Evidently, the non-equilibrium model seems capable of effectively capturing non-Newtonian viscosity data by adjustment of just one parameter.

The results from the acoustic measurements are presented in Fig. 2.8. The observed effect of strain rate on shear modulus has also been seen in recent molecular dynamics simulations [37]. In Fig. 2.8 we superimpose the shear moduli predicted from viscosities using Eq.(2.3), along with the solution of the non-equilibrium law, Eq. (2.4). As evidenced from Fig. 2.8, the shear modulus measured acoustically can be adequately correlated to the measured viscosity. The small apparent discrepancy in this correlation may be related to the *ex situ* nature of the acoustic experiment. During unloading and quenching of specimens prior to measuring sound velocities, some degree of relaxation towards equilibrium might occur, or some fraction of the potential energy might instantaneously recover as elastic energy, resulting in lower apparent strain-rate sensitivity.

We have therefore demonstrated that liquid fragility and strain-rate sensitivity are dictated by the softening of W, which is uniquely determined by the thermodynamics of G. We can therefore regard G as the effective thermodynamic state variable governing

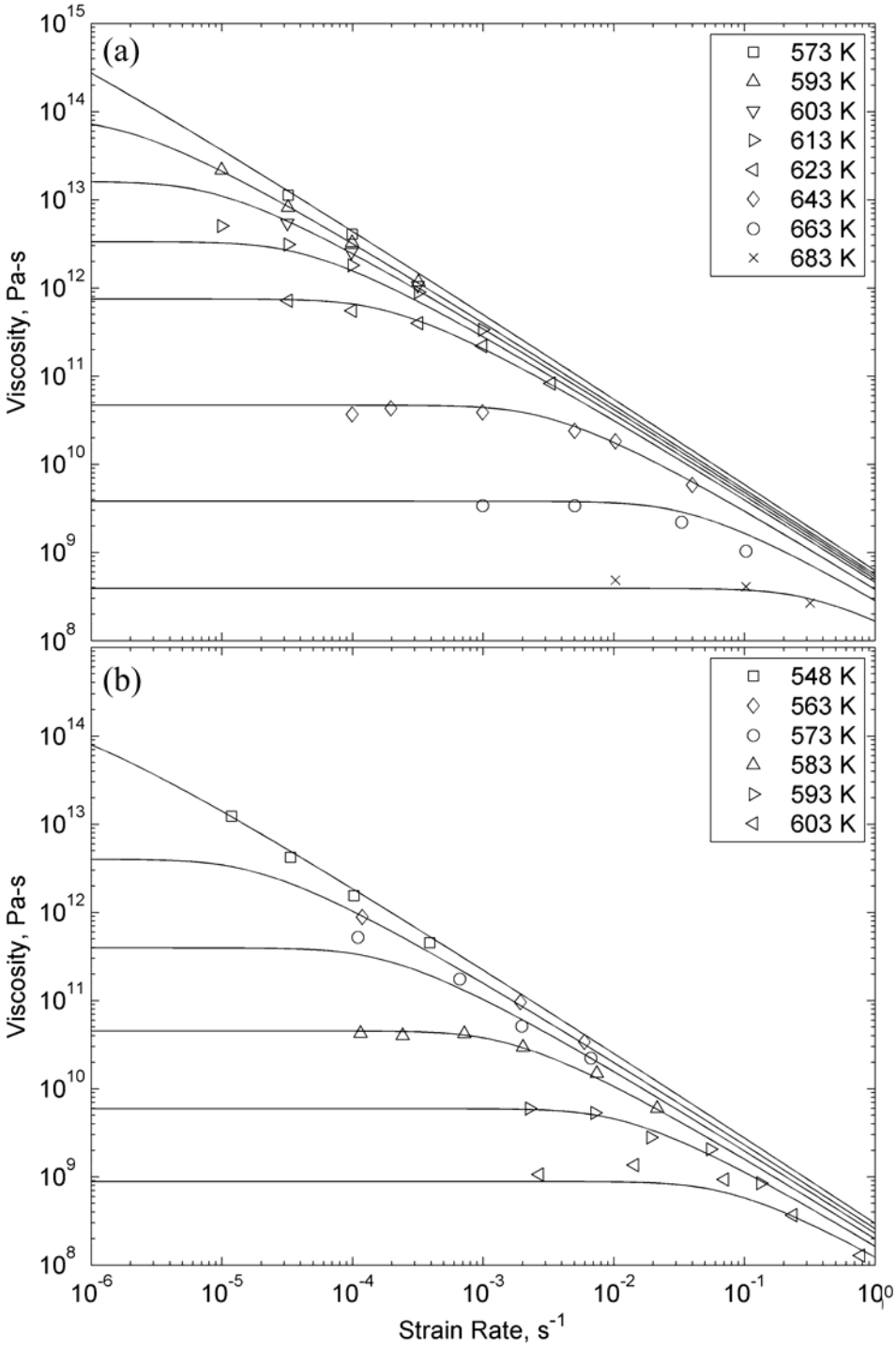

Figure 2.7. Fit of the non-equilibrium viscosity law, Eq. (2.4), to the non-Newtonian data of (a) $Zr_{41.2}Ti_{13.8}Ni_{10}Cu_{12.5}Be_{22.5}$ [28], and (b) $Pd_{40}Ni_{10}Cu_{30}P_{20}$ [14]. The data was obtained by continuous-strain-rate compression experiments using the Instron setup described in [28]. The small discrepancy in the Newtonian data of $Zr_{41.2}Ti_{13.8}Ni_{10}Cu_{12.5}Be_{22.5}$ between [28] and [8] was adjusted by introducing a temperature correction of 8 K.

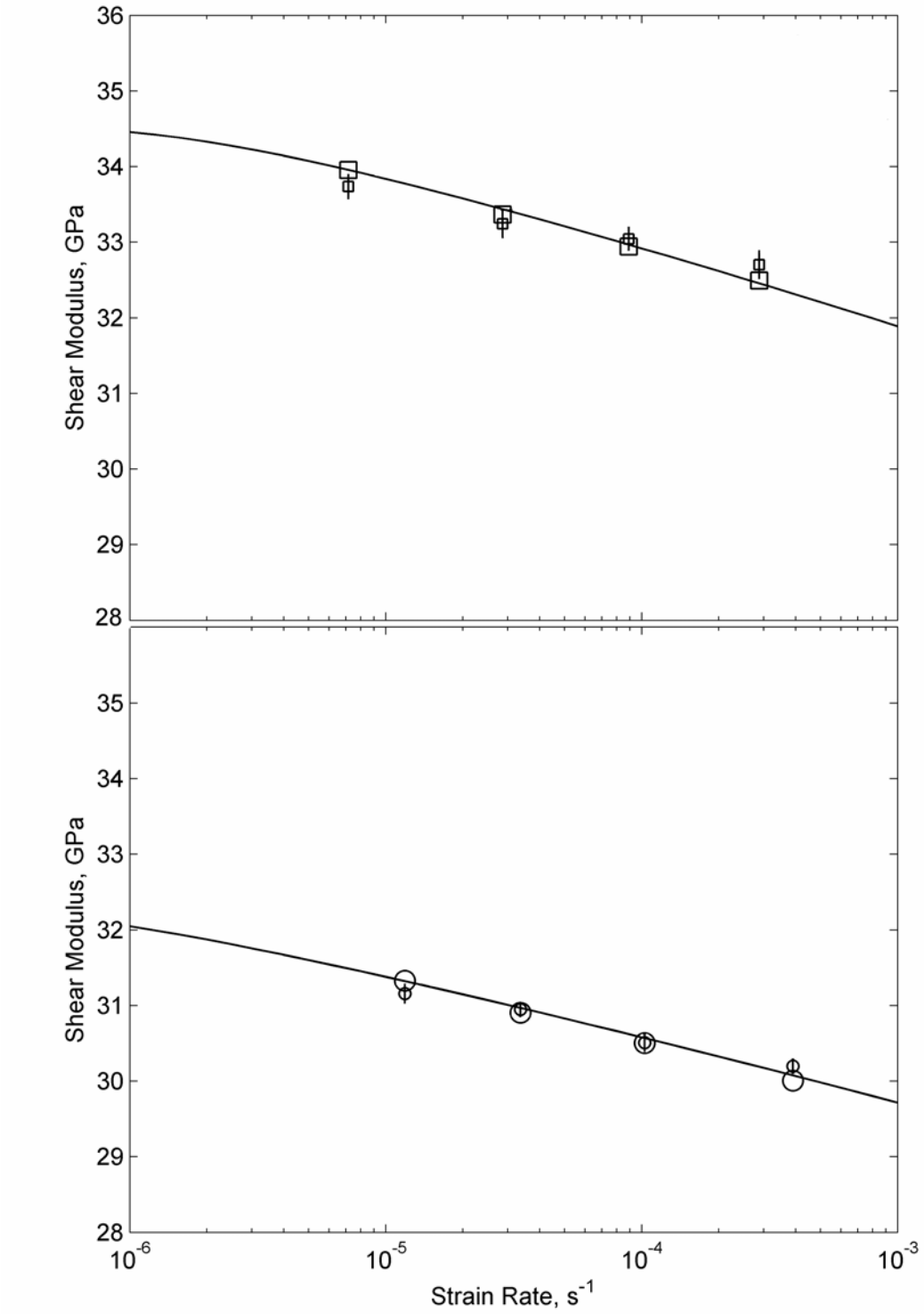

Figure 2.8. Acoustically measured shear moduli (corrected for Debye-Grüneisen effect) of quenched unloaded specimens following steady deformation at the indicated rates: $Zr_{41.2}Ti_{13.8}Ni_{10}Cu_{12.5}Be_{22.5}$ at 593 K (□) and $Pd_{40}Ni_{40}P_{20}$ at 548 K (○). Shear modulus predicted from viscosity data using Eq. (2.3): $Zr_{41.2}Ti_{13.8}Ni_{10}Cu_{12.5}Be_{22.5}$ at 593 K (☐) and $Pd_{43}Ni_{10}Cu_{27}P_{20}$ at 548 K (○). Solid lines are predictions from Eq. (2.4).

flow. Contrary to free volume, which is presumed to vanish at some finite temperature below the glass transition producing a singularity in viscosity, G is measurable and is thermodynamically well behaved, rendering the viscosity law thermodynamically consistent. Fundamentally, G represents the isoconfigurational shear modulus of the liquid at the high-frequency "solid-like" limit, and, unlike free volume, is a thermodynamically well defined and experimentally accessible property. Accordingly, *in situ* ultrasonic acoustic measurements during mechanical deformation would be expected to correlate with viscosity assessed from measuring flow stress. We shall hence attempt to validate such correlation by measuring ultrasonic shear moduli of stressed configurational states and comparing them to the associated viscosities.

2.5 Conclusion

In conclusion, we performed viscosity measurements on $Pd_{43}Ni_{10}Cu_{27}P_{20}$ and isoconfigurational shear modulus experiments on $Zr_{41.2}Ti_{13.8}Ni_{10}Cu_{12.5}Be_{22.5}$ and $Pd_{43}Ni_{10}Cu_{27}P_{20}$. Furthermore, we presented a rheological law based on the concept of cooperatively sheared flow zones, in which the effective thermodynamic variable governing flow is identified to be the isoconfigurational shear modulus of the liquid. The model was capable of explaining the equilibrium as well as the non-equilibrium flow of metallic-glass-forming liquids.

We successfully applied this model to alloys with different fragilities. This included the $Zr_{41.2}Ti_{13.8}Ni_{10}Cu_{12.5}Be_{22.5}$, $Pd_{40}Ni_{40}P_{20}$, $Pd_{40}Ni_{10}Cu_{30}P_{20}$, $Pd_{77.5}Cu_{6}Si_{16.5}$, $La_{55}Al_{25}Ni_{20}$, and $Mg_{65}Cu_{25}Y_{10}$ alloys. In all cases the fits worked equally well in the high- and low-temperature regimes. Additionally, the one-parameter fit is found to be as good as the three-parameter Cohen-Grest Law.

In addition to the viscosity fits, we compared the shear moduli obtained by experiment and shear moduli calculated from viscosity for different strain rates. It was shown that there was a good correlation between the measured and calculated shear moduli. The model was also found to fit Newtonian data over a wide range of temperatures. This suggests that the assumption of a unique function of shear modulus with temperature is valid. Therefore, we have demonstrated that variations in viscosity with both temperature and strain rate can be uniquely correlated to variations in isoconfigurational shear modulus, and hence verified that viscosity has a unique functional relationship and a one-to-one correspondence with shear modulus.

2.6 References

[1] W H Wang, C Dong, and C H Shek, Mat. Sci. and Eng. R 44, 45 (2004).

[2] J Lu, Ph.D. Thesis. Pasadena: California Institute of Technology (2002).

[3] F. Spaepen, Acta Metall. 25, 407 (1977).

[4] A. S. Argon, Acta Metall. 27, 47 (1979).

[5] K. M. Flores, D. Suh, and R. H. Dauskardt, J. Mater. Res. 17, 1153 (2002).

[6] K. Hajlaoui, T. Benameur, G. Vaughan, and A. R. Yavari, Scripta Mater. 51, 843 (2004).

[7] W. L. Johnson, and K. Samwer, Phys Rev. Lett. 95, 195501 (2005).

[8] J. Frenkel, Z. Phys. 37, 572 (1926).

[9] N Nishiyama, and A Inoue, Mat. Tran. JIM 37, 1531 (1996).

[10] A Peker, and W L Johnson, Appl. Phys. Lett. 63, 2342 (1993).

[11] J. Markus, and V. Zuluff, Handbook of industrial electronic control circuits, New York: McGraw-Hill (1959).

[12] M Yamasaki, S Kagao, Y Kawamura, and Y K, Appl. Phys. Lett. 84, 4653 (2004).

[13] G J Fan, J F Löffler, and R K Wunderlich, Acta Mater. 52, 667 (2004).

[14] E. Screiber, O. Anderson, and N. Soga, Elastic Constants and their Measurement, McGraw-Hill (1973).

[15] M. L. Lind, G. Duan, and W. L. Johnson, Phys. Rev. Lett. 97, 015501 (2006).

[16] N. Nishiyama, A. Inoue, and J. Z. Jiang, Appl. Phys. Lett. 78, 1985 (2001).

[17] A. Masuhr, T. A. Waniuk, R. Busch, and W. L. Johnson, Phys. Rev. Lett. 82, 2290 (1999).

[18] J. Lu, G. Ravichandran, and W. L. Johnson, Acta Mater. 51, 3429 (2003).

[19] H Kato, T Wada, M Hasegawa, J Saida, A Inoue, and H S Chen, Scripta Mater. 54, 2023 (2006).

[20] H Kato, Y Kawamura, A Inoue, and H S Chen, Appl. Phys. Lett. 73, 3665 (1998).

[21] G. H. Fan, H.-J. Fecht, and E. J. Lavernia, Appl. Phys. Lett. 84, 487 (2004).

[22] W. L. Johnson, unpublished.

[23] K. H. Tsang, S. K. Lee, and H. W. Kui, J. Appl. Phys. 70, 4837 (1991).

[24] G. Wilde, G. P. Gorler, K. Jeropoulos, R. Willnecker, and H. J. Fecht, Mater. Sci. Forum 269-272, 541 (1998).

[25] Y. Kawamura, and A. Inoue, Appl. Phys. Lett. 77, 1114 (2000).

[26] C. A. Angell, Science 267, 1924 (1995).

[27] H. S. Chen, J. Non-Cryst. Solids 27, 257 (1978).

[28] I. Egry, G. Lohofer, I. Seyhan, S. Schneider, and B. Feuerbacher, Int. J. Thermophys. 20, 1005 (1999).

[29] Y. Kawamura, T. Nakamura, H. Kato, H. Mano, and A. Inoue, Mater. Sci. Eng. A304-306, 674 (2001).

[30] T. Yamasaki, T. Tatibana, Y. Ogino, and A. Inoue, in Proceedings of the 1998 MRS Fall Meeting, Materials Research Society, edited by C. T. L. W. L. Johnson, and A. Inoue (Warrendale, PA, 1999) p. 63.

[31] S.-S.Wu, T.-S. Chin, K.-C. Su, and F.-H. Shyr, Jpn. J. Appl. Phys. 35, 175 (1996).

[32] R. Busch, W. Liu, and W. L. Johnson, J. Appl. Phys. 83, 4134 (1998).

[33] H. Vogel, Z. Phys. 22, 645 (1921).

[34] M. H.Cohen, and G. S. Grest, Phys. Rev. B. 20, 1077 (1979).

[35] R. Busch, Y. J. Kim, and W. L. Johnson, J. Appl. Phys. 77, 4039 (1995).

[36] X. Hu, Y. Li, S. C. Ng, and Y.P. Feng, Phys. Rev. B 62, 3169 (2000).

[37] M. Zink, K. Samwer, W. L. Johnson, and S. G. Meyer, Phys. Rev. B (In Press).